Post-launch ICESat Science Team Contributions by the Laboratories for Space Geodesy and Planetary Geodynamics at NASA's Goddard Space Flight Center

David Harding, Scott Luthcke, David Rowlands, Jeanne Sauber, Claudia Carabajal, and Teresa Williams

February 1, 2005

This document describes post-launch contributions to the ICESat Science Team by members of Laboratories for Space Geodesy (Code 697) and Planetary Geodynamics (Code 698) within the Solar System Exploration Division at NASA's Goddard Space Flight Center. Prior to January, 2005 these organizations were branches within the Laboratory for Terrestrial Physics (LTP). The work by this group was initiated by Jack Bufton, ICESat Science Team member and former LTP Associate Chief for Sensors. Summaries are provided for contributions in two areas, Data Calibration and Validation, and Science Applications. Additional contributions in the areas of Instrument Operations, Data Processing and Visualization, and External Collaborations and Student Training are also listed.

Contents

1. Data Calibration and Validation Contributions

1.1 Calibration and Reduction of ICESat Geolocation Errors for Change Detection

1.1.A. Analysis and results

The accurate horizontal and vertical geolocation of the ICESat Geosciences Laser Altimeter System's (GLAS) surface returns is a critical issue in the scientific application of these data. Laser pointing, ranging, timing and orbit errors must be compensated to accurately geolocate the laser altimeter surface returns. Towards this end, we have exploited the laser range observations in an integrated residual analysis to accurately calibrate these geolocation/instrument parameters *[Luthcke et al., 2002, 2003a, 2003b]*. Although we have applied our techniques to the recovery of all geolocation/instrument parameters (pointing, ranging, timing and orbit), currently pointing errors, and errors that manifest themselves as pointing (e.g. field of view shadowing), represent the dominant geolocation error source. Furthermore, pointing errors directly impact the calibration of other geolocation parameters (e.g. range biases). Therefore, the results and analysis presented here concentrate on the calibration and correction of pointing errors. The ICESat laser altimeter data have been processed as direct altimetry from ocean scans (OS) and "round"-the-world scans (RTWS - continuous OSs for an orbit revolution) along with dynamic crossovers in order to calibrate, correct and validate laser pointing biases, along with complex long-period and orbital period variation. These scans are special spacecraft maneuvers that we have designed to calibrate pointing errors as accurately as possible *[Luthcke et al., 2000]*.

Figure 1 presents the OS and RTWS range residual pointing calibration results for two representative laser operation periods (L2A and L3A) using release 18 of the ICESat data products. Laser operations period 2A (L2A) represents our best performing time period where full Stellar Referencing System (SRS) pointing corrections were available and applied. Due to instrument specific problems, full SRS data is not available for laser operations period L3A. The OS and RTWS range residual pointing recovery ("effective pointing") accounts for both transmit and receiver effects such as field of view (FOV) shadowing, while the SRS accounts for transmit effects. Individual OS range residual analysis pointing calibration results (left in Figure 1) and orbital pointing variation recovered from RTWS range residual analysis (right in Figure 1) demonstrate there are significant long-period and orbital effective pointing variations remaining in the data. These remaining effective pointing errors induce significant time varying, geographically correlated systematic geolocation errors, adversely impacting such analysis as change detection and range bias estimation.

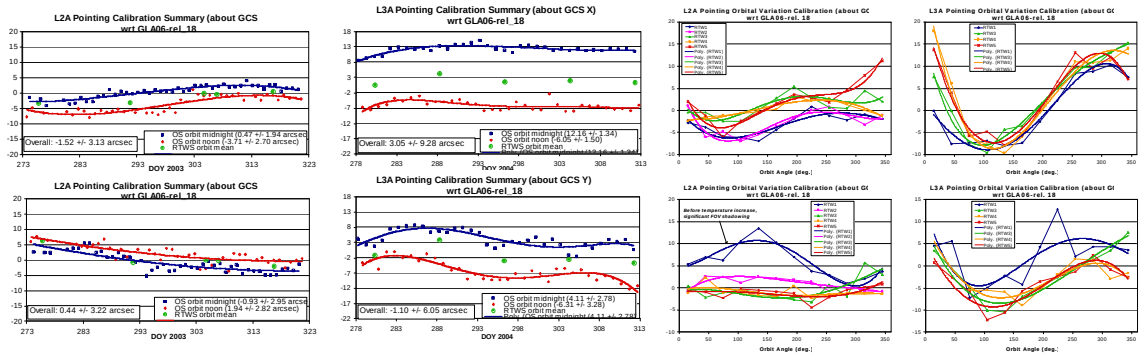

Figure 1. L2A and L3A time-varying bias and orbital variation calibration using release 18 data.

The calibration results shown in Figure 1 have been used to develop functional corrections for the observed time varying bias and orbital variations for both the L2A and L3A periods. These "effective pointing" corrections account for both transmit and receiver effects, such as field of view (FOV) shadowing. For a first attempt at this correction, we have applied a first iteration solution for the time varying bias and a single average orbital variation correction for each observation period. The current correction solution (corrv2) results in significant geolocation accuracy improvement as shown in Figures 2 and 3. Improvement in Greenland and Antarctica crossover residual statistics are shown in Figure 2. The Greenland and Antarctica data were not used in the development of the corrections and provide an independent assessment. The effective pointing corrections result in significant improvement in geographically correlated error as shown in the Antarctica crossover residuals averaged in 5 degree bins (Figure 3).

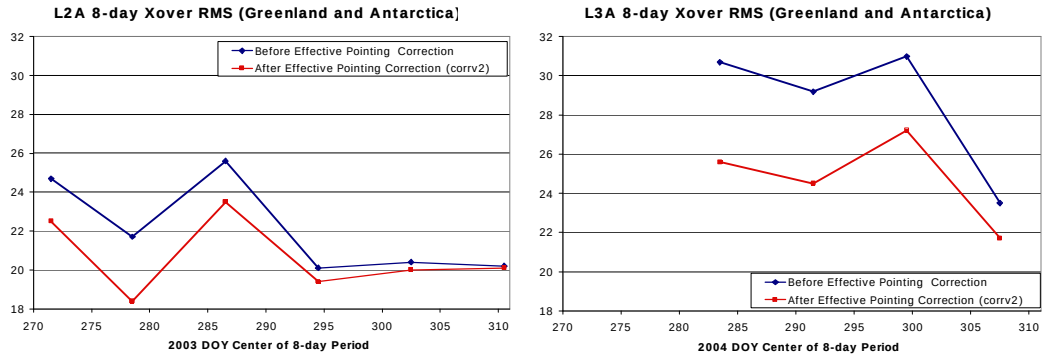

Figure 2. Improvement in Greenland and Antarctica release 18 crossover discrepancies.

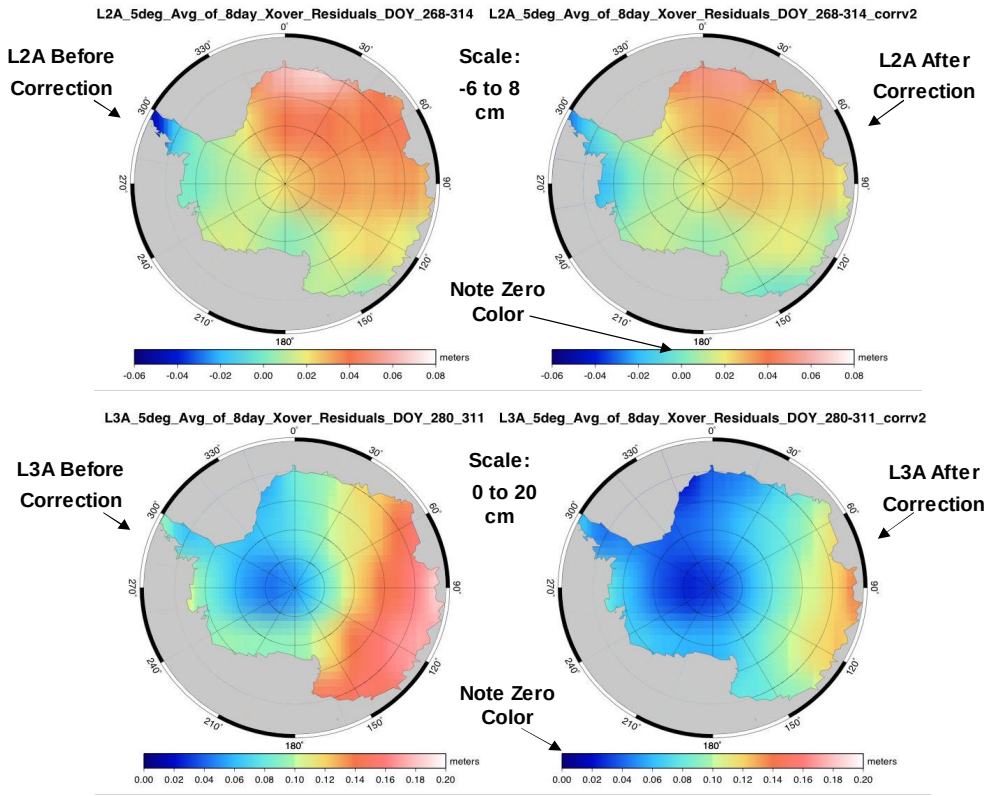

Figure 3. Reduction of geographically-correlated release 18 crossover discrepancies.

We are currently refining this analysis and correction technique using release 19 of the ICESat data products. Release 19 includes an Instrument Star Tracker (IST) distortion correction that accounts for high-frequency attitude error. The elimination of this high-frequency IST error has improved our calibrations. Therefore, initial results from our new L2A calibrations and correction show still further improvement over the results shown here using this initial release 18 data analysis *[Luthcke et al., 2005]*. For example ice sheet crossovers, computed using L2A release 19 days 275-282, improve from 19.2 cm RMS to 14.6 cm RMS using our effective pointing corrections. This would then suggest the corrected data is meeting the 11 cm elevation accuracy mission requirement, assuming the errors in the crossing tracks are independent. We are in the process of further validation and then final application of these corrections into a new release 20 ICESat data product for each observation period. With these effective pointing corrections applied, the elevation accuracy for each observation period is expected to meet the initial mission requirement.

1.1.B. GEODYN algorithm and software development

In order to perform the above calibration, correction and error analysis, extensive GEODYN algorithm and software development has been performed. GEODYN is an orbit determination and geodetic parameter estimation software package. It accepts a wide range of tracking data types including altimetry. Although GEODYN is developed and maintained in the Laboratory for Space Geodesy (Code 697) at NASA's Goddard Space Flight Center, it is distributed to various university and government research groups.

GEODYN has the ability to use laser altimetry in the form of ranges to the Earth's surface (direct altimetry) and also in the form of crossover constraint equations to estimate parameters. GEODYN's already existing laser altimetry capability was expanded for the ICESat mission. As a result, GEODYN is used by the ICESat mission to determine sub-arcsecond laser pointing corrections in roll and pitch. The infrastructure and experience gained from ICESat will benefit future altimeter missions.

Because ICESat measures attitude at laser observation epochs, GEODYN was upgraded to use attitude information taken directly at observation times (as opposed to interpolating at measurement times). This reduces the effect of jitter. Also, because biases in pointing are likely caused by thermal effects and therefore unlikely to remain constant over any significant period of time, GEODYN was given the ability to estimate a wide range of time dependent pointing parameters. With this suite of parameters, we were able to account for the time varying pointing biases and orbital variations induced by thermal mechanical variation, as discussed above.

1.2 Profile Matching for Geolocation Validation

To validate the horizontal accuracy of geolocation solutions derived by the integrated residual analysis method, we have developed a procedure for matching elevation profiles to Digital Elevation Models (DEMs) with moderate resolution (10 to 90 m) for areas with rugged topographic relief *[Rowlands et al. (2000), Luthcke et al. (2002)]*. Footprint elevations are differenced with the corresponding DEM value, and the standard deviation of the differences establishes a residual for the profile as a whole. As profiles are systematically shifted over the DEMs, the proper geolocation of the profile is established by the location of the residual minima (Figure 4). We are applying this approach using U.S. National Elevation Data DEMs produced by the U. S. Geological Survey and Shuttle Radar Topography Mission (SRTM) DEMs produced by a joint NASA-NGA mission. The method has documented the increasing improvement in ICESat geolocation accuracy as refined calibrations and new data releases are produced *[Carabajal et al., 2003]*. The geolocation accuracy of the upcoming release 20 product, which will incorporate full pointing calibration corrections, will be systematically assessed with this method.

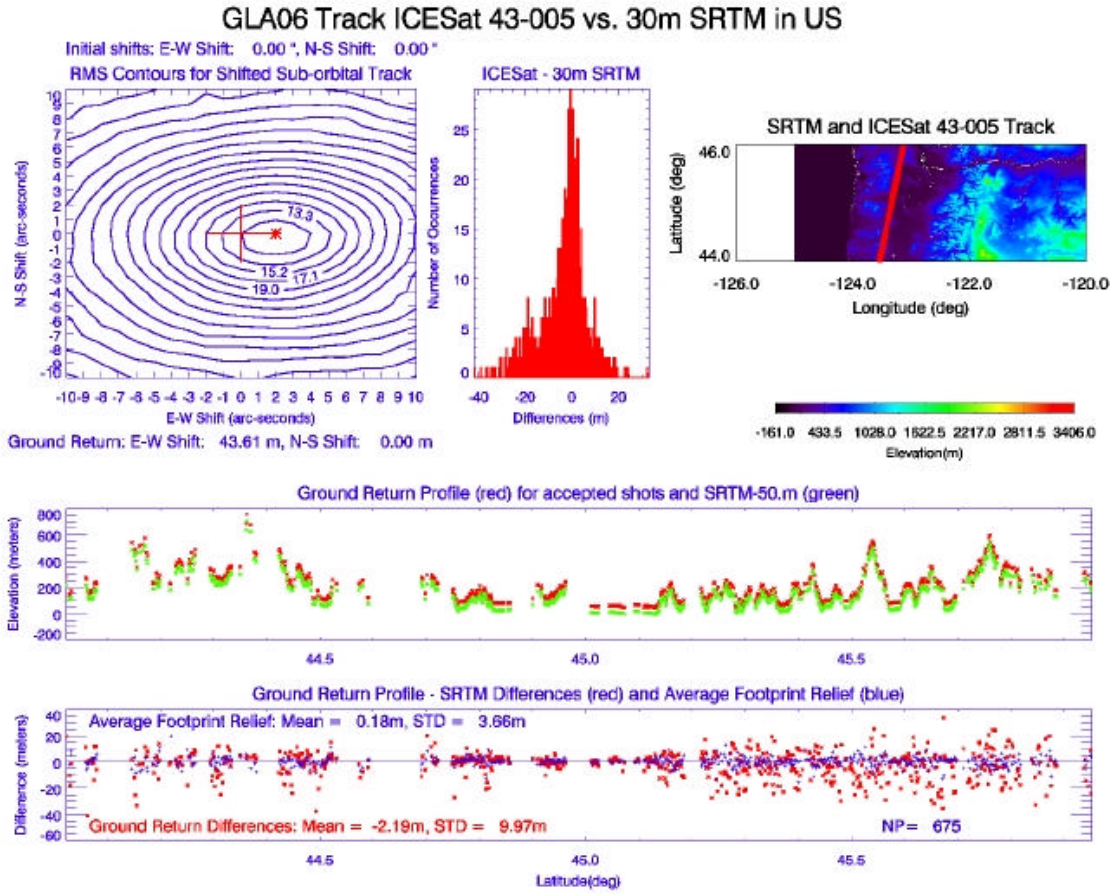

Figure 4. Profile matching result for an ICESat track in the U.S. Pacific Northwest, with contours of elevation residuals (upper left) indicating that the location of best match (red asterisk) to a 30 m resolution SRTM DEM requires an approximately 40 m westward shift of this preliminary ICESat geolocation result. Elevation differences between ICESat and the DEM at the location of best match are shown in profile (red, bottom) and as histogram (center top).

1.3 Waveform Matching for Land Products Validation

ICESat altimeter channel waveforms measure within-footprint relief due to ground slope and roughness, structures and vegetation cover. In order to validate waveform-derived elevation parameters, such as highest, average, and lowest illuminated surfaces within laser footprints, as well as footprint geolocation results, we have developed a grid-based waveform simulation capability to compare observed ICESat waveforms to synthetic waveforms produced from high resolution (1-5 m) Digital Elevation Models (DEMs) *[Harding and Carabajal, 2005]*. We simulate the instrument's response to complex topographic surfaces, including the laser far-field energy pattern, boresight field-of-view alignment, and detector impulse response. Comparison to synthetic waveforms derived from high-resolution airborne laser mapping data demonstrates that ICESat waveforms provide detailed and accurate information on the within-footprint distribution of surface heights (Figure 5). In addition, the location of maximum correlation between observed and computed waveforms provides a high-resolution assessment of geolocation accuracy on a footprint-by-footprint basis. We are now applying this simulation capability to assess ranging errors due to waveform distortion introduced by atmospheric forward scattering, waveform saturation, and field-of-view shadowing.

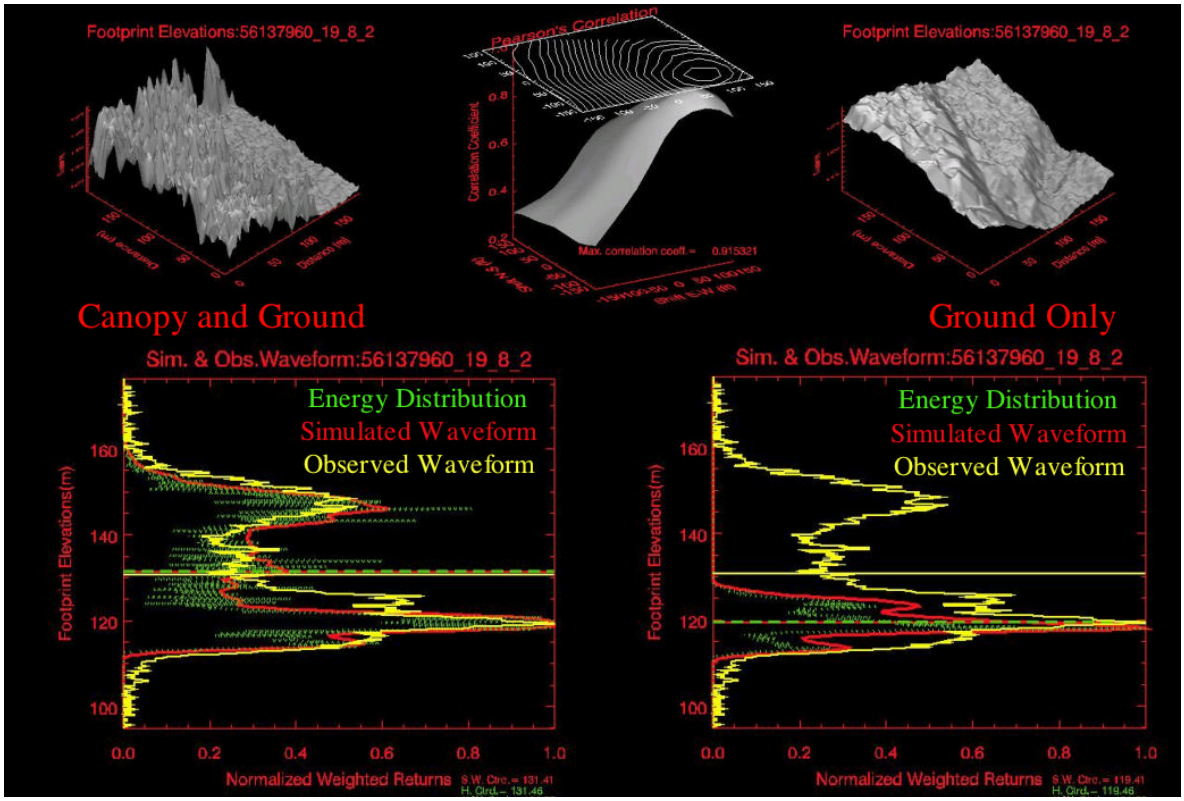

Figure 5. ICESat waveform (yellow) from a vegetated landscape compared to a DEM-derived waveform simulation of the canopy and ground surface (red, left), at the location of best-match where correlation is maximized (top center), and a ground-only simulation with vegetation removed (red, right). Perspective views show the canopy and ground (upper left) and ground-only (upper right) DEM surfaces at the footprint location.

2. Science Application Contributions

2.1 Integration of ICESat and SRTM Land Topography Data

Understanding the quality of land topography data sets, as represented in Digital Elevation Models (DEMs), is crucial to their use in land process studies and in detection of topographic changes obtained from comparison of DEMs acquired at different times. ICESat elevation data provides a globally distributed data set of very high accuracy that is being used to independently estimate the vertical accuracy of continental DEMs with 30 m and 90 m spatial resolution produced by the joint NASA-NGA Shuttle Radar Topography Mission (SRTM). We have documented elevation differences between ICESat and SRTM C-band elevations for various regions of the world with variable topography and vegetation cover *[Carabajal and Harding, 2005]*. In vegetated regions, ICESat data enables the estimation of radar phase center elevation biases with respect to top of canopy, waveform centroid, and underlying ground. Correlations of ICESat to SRTM elevation differences have been established with local relief, land cover, waveform extent, a surrogate for canopy height, and waveform relative centroid height, a surrogate for canopy closure. Regional analyses have been conducted in southern Alaska, the U.S Pacific Northwest (Figure 6), Amazonia, East Africa, Tibetan Plateau, Himalayan Mountains, and western Australia. Future ICESat data product releases will include the SRTM elevation and local relief for each laser footprint location, facilitating global analyses using these complimentary elevation measurement systems. This combination of ICESat and SRTM will produce the most accurate global land topographic data available for the Earth.

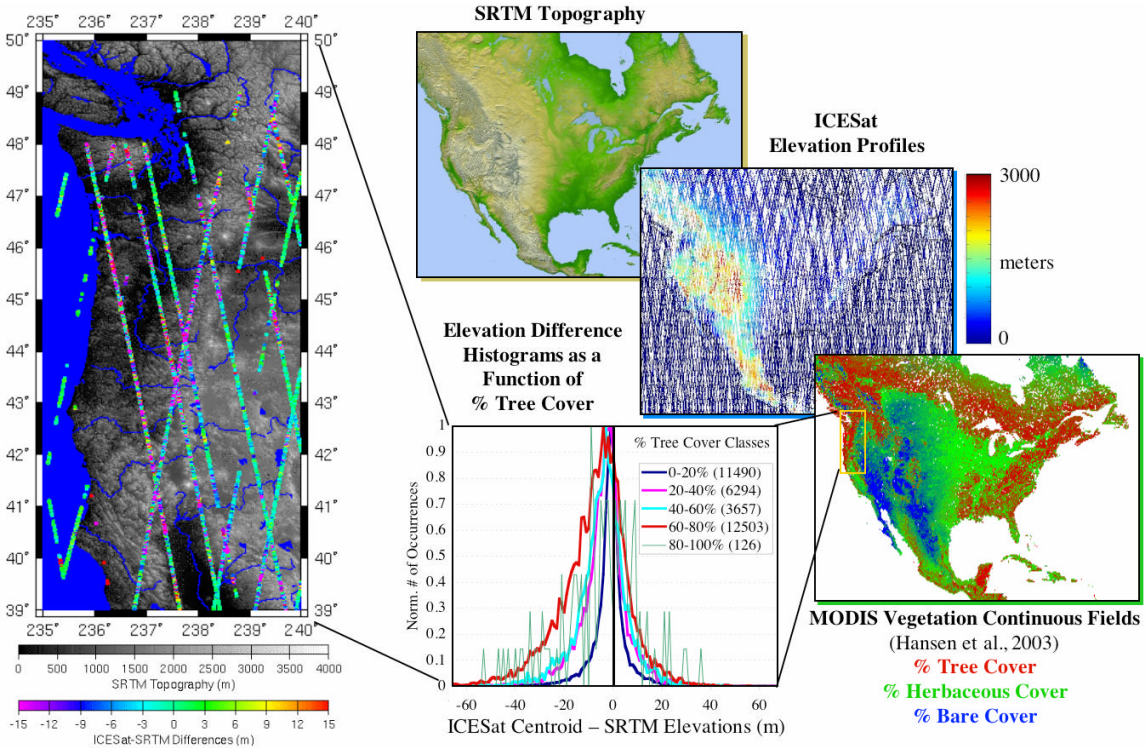

Figure 6. Histograms of elevation difference between the ICESat waveform centroid and SRTM in the U.S. Pacific Northwest; SRTM C-band phase center elevations become upward biased and less accurate as tree cover percentage, derived from MODIS images, increases.

2.2 Vegetation Height and Biomass from Combined ICESat and SRTM Data

Although the exchange of carbon between the atmosphere and forested ecosystems is a vital component of the global carbon cycle, it is a portion of the cycle that is not well-characterized nor well-understood. Lidar remote sensing has a unique capability for estimating forest canopy height, which has a direct and increasingly well-understood relationship to aboveground carbon storage *[e.g. Lefsky et al, 2002]*. While ICESat has collected an unparalleled data set of lidar waveforms over terrestrial targets, processing of GLAS data to create reliable estimates of forest height is complicated by sloped-ground surfaces within the large diameter ICESat footprint that cause waveform broadening and a resulting overestimate of vegetation height. With external collaborators, a method has been developed to correct this broadening effect using SRTM data to quantify local relief at ICESat footprint locations *[Lefsky et al., 2005]*. Biome-specific regression of estimated tree height, based on ICESat waveform width and SRTM local relief, versus maximum tree height observed in 63 field plots in three biomes (Amazonia and the U.S. Southeast and Pacific Northwest) yields a prediction of 74% of the observed variance (Figure 7, left). For the Amazon plots, estimated tree height accounts for 74% of the variance in aboveground biomass, derived from field measurements of stem diameter and tree height (Figure 7, right). The linear regression relationship applies to stands having a broad range of aboveground biomass, unlike passive optical and radar backscatter methods that become insensitive for stands of moderate to high biomass. Aboveground biomass results for the U.S. Southeast and Pacific Northwest are in progress. These initial results demonstrate that combined ICESat and SRTM data has the potential to provide global inventory data on forest height and aboveground biomass with accuracies significantly exceeding other currently available satellite-based observations.

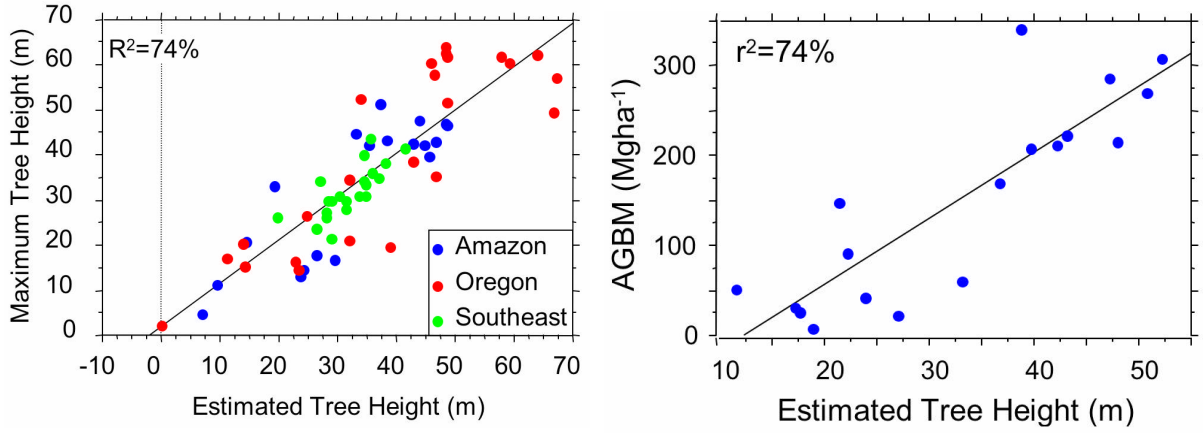

Figure 7. Regressions of estimated tree height predicted from ICESat waverform width and SRTM local relief versus maximum tree height (left) and aboveground biomass (right) in field plots located at ICESat footprint locations.

2.3 ICESat Observations of Inland Surface Water Stage and Slope

River discharge and changes in lake, reservoir and wetland water storage are critical terms in the global surface water balance, yet they are poorly observed globally and the prospects for adequate observations from in-situ networks are poor. Measurements of water surface height (stage), slope, and extent provide a means to remotely monitor inland water storage and river discharge. ICESat data are being used to demonstrate the potential for satellite laser altimetry measurements of these inland water parameters and their contribution to global water balance monitoring *[Harding and Jasinski, 2004]*. For example, exact-repeat profiling of a portion of the lower Mississippi River on three dates documents river stage and slope measurement precision of 10 cm and 1 cm per km at and between crossings of channel meanders, respectively (Figure 8, upper right). Changes in ICESat-derived stage, average slope of the reach, and local slopes between meander crossings are observed between the three profiles, and the stage changes correlate with in-situ gage measurements (Figure 8, lower). Continuing work is documenting stage and slope retrieval capabilities as a function of cloud cover (frequency and optical depth) and return signal strength (dependent on off-nadir angle and water roughness).

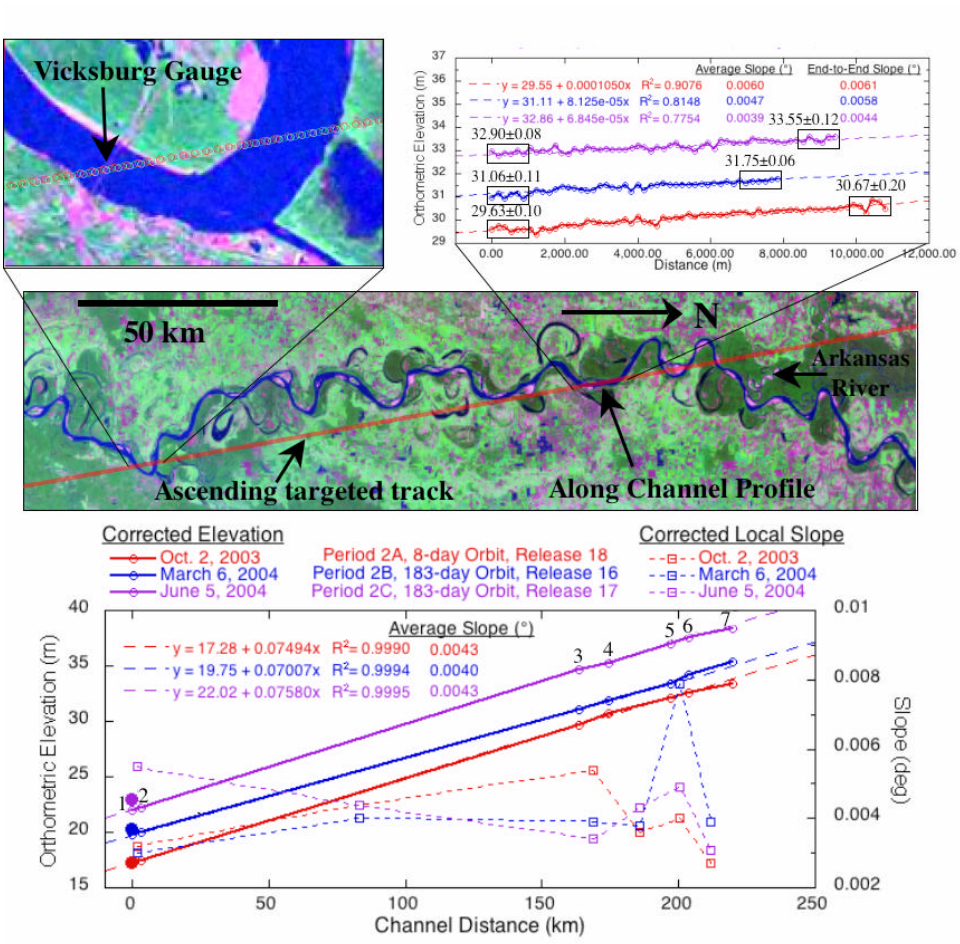

Figure 8. Three repeated ICESat elevation profiles targeted on the Mississippi River between Vicksburg, MS and the confluence with the Arkansas River plotted on a false-color Landsat Thematic Mapper image. Labels 1 through 7 in the lower panel indicate the locations where the profiles intersect the river. Solid circles between locations 1 and 2 are in-situ river stage measurements at the times of the ICESat profiles.

2.4 ICESat Results for Southern Alaska Glaciers

The glaciers of the southeastern Alaska coastal region are the largest temperate glacier meltwater source on Earth and may contribute one third of the total glacier meltwater entering the global ocean. Since melt onset and refreeze timing in this region shows a tendency toward earlier onset and longer ablation seasons, accelerated glacier wastage may be occurring [*Ramage and Isaacs*, 2003; *Arendt et al., 2002*]. Mountain glaciers generally have rougher surfaces and steeper regional slopes than the ice sheets for which the ICESat design was optimized. However we found that by working with well-located individual returns, combined with earlier geodetic data, we could use ICESat to estimate short-term elevation change and ice change over the last decade. In three studies we report elevation changes on two of the largest temperate glacier systems on Earth, the Bering Glacier and the Malaspina Glacier systems (Figure 9). Additionally we examined the relation between melting glaciers, earthquake faulting, and earthquake hazard in this same region.

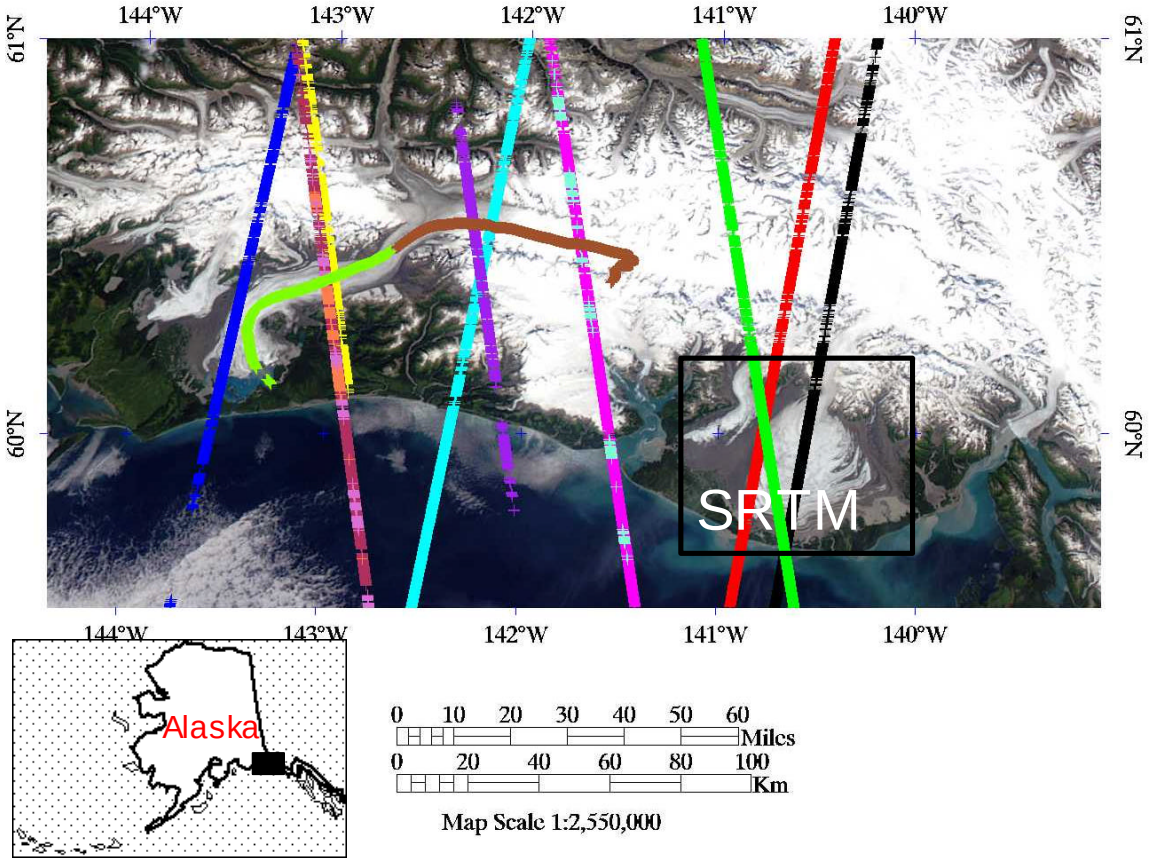

Figure 9. The Moderate Resolution Imaging Spectroradiometer (MODIS) image shows the location of the Malaspina Glacier in the east and the Bering Glacier piedmont lobe in the west. Bagley IV=Bagley Ice Valley, IB=Icy Bay, YB=Yakutat Bay. Ascending ICESat tracks = SE to NW trending lines, descending ICESat tracks = NE to SW trending lines. The location of Echelmeyer's 1995 aircraft observations on the Bagley IV (brown) and Bering Glacier piedmont lobe (bright green). The black box shows the study region on the outline of Alaska.

2.4.a. Wastage of the Malaspina Piedmont Lobe: SRTM versus ICESat (2000-2004)

Sauber et al., [2005] report and interpret ice elevation change between a digital elevation model (DEM) derived from the Shuttle Radar Topography Mission (SRTM C-band) observations in Feb. 2000 and ICESat Laser 1-3 observations between Feb. 2003 and Nov. 2004. Between 2000 and 2004 ice elevation decreases of 10-30 meters occurred across the central Malaspina piedmont lobe (Figure 10).

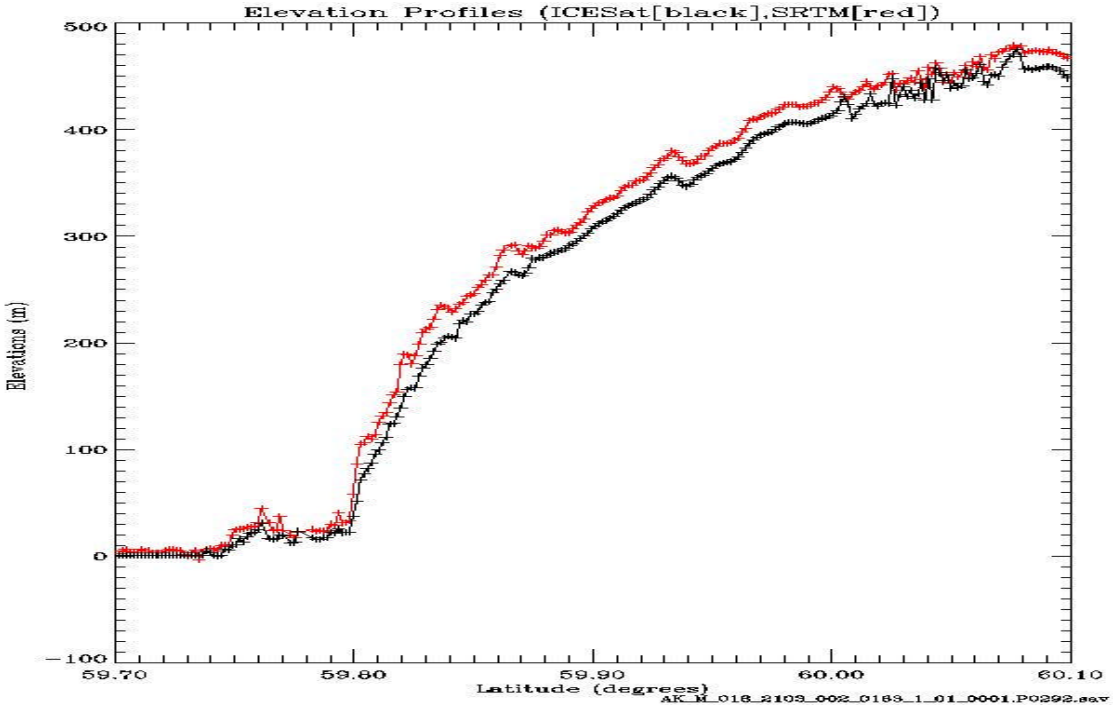

Figure 10. Shuttle Radar Topography Mission (SRTM, in red) and ICESat (black) elevations across the central Malaspina piedmont lobe (black descending ICESat track given in Figure 9).

2.4.b. Elevation change in the Bagley Ice Valley and Bering Glacier piedmont lobe: aircraft laser altimetry versus ICESat (1995-2004)

Ongoing retreat of the Bering Glacier since 1905 has been interrupted at least six times by glacier surges. *Sauber et al., [2004]* used aircraft laser altimetry measurements made in 1995 by *Echelmeyer et al., [2002 NSIDC notes, see also Arendt et al., 2002, Echelmeyer et al., 1996]* and ICESat measurements in 2003/2004 to estimate the elevation changes in the surge reservoir and receiving area following the most recent (1993-1995) surge. Between 1995 and 2004 we estimated >10 meters of elevation increase occurred in the Bagley Ice Valley accumulation region (Figure 11) and in the upper reaches of the Bering Glacier piedmont lobe the surface elevation decreased by 27 meters.

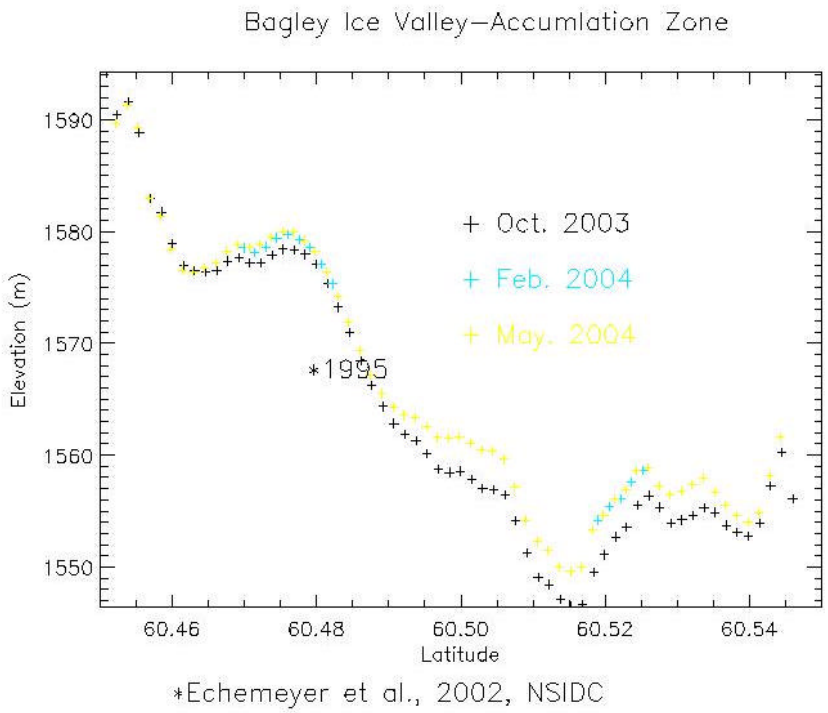

Figure 11. Elevation versus latitude along ICESat exact repeat tracks (ascending purple track given in Figure 9) that intersects with the aircraft laser altimetry (given by a *) of *Echelmeyer et al., [2002]*.

2.4.c. Winter elevation increase (2003/2004) from sequential ICESat measurements across the the snow accumulation regions on the Bagley Ice Valley and Seward Glacier

Few direct glaciological observations are available for the source region of the large Alaska glaciers. Snow accumulation rates have been largely inferred from low-altitude precipitation and temperature data. Comparing sequential ICESat observations in the Malaspina source region (Seward Glacier), we estimated short-term elevation increases of up to 5 meters during the winter of 2003/04. In the Bagley Ice Valley, the snow accumulation was ~3 meters in the flat regions (Figure 11).

2.4.d. Melting glaciers, earthquake faulting and hazard

The rapid wastage of southern Alaska glaciers occurs in a region under going rapid tectonic strain accumulation *[Sauber et al., 2000; Sauber and Molnia, 2004]*. We are using ICESat observations, along with earlier geodetic data, to estimate the temporal and spatial fluctuations in ice mass, to evaluate their influence on earthquake hazard, and to identify surface offset features due to earthquake faulting. For example, some surface features of the Malaspina Glacier observed with ICESat may be correlated with the seismically active Malaspina fault *[Wiest et al., 2004]*.

2.5 Ice Sheet Mass Change from a Combination of ICESat and GRACE Data

A major goal of the ICESat mission and the NASA Oceans and Ice Program is to investigate and monitor ice sheet mass balance on scales that significantly affect sea level. Along with ICESat's observations of surface height change, the GRACE mission's ultra-precise inter-satellite range and range rate measurements provide a complementary form of remote sensing with their ability to detect gravity (mass) change. By its very nature, temporally varying surface height, *dh/dt*, obtained from altimetry is a boundary condition that has a somewhat ambiguous relationship to the underlying mass flux. In addition, altimeter data acquired over specific narrow surface transects require spatial filtering and interpolation to deduce height changes over broader regions. The simultaneous determination of height and gravity from the ICESat and GRACE missions can reduce many of the ambiguities associated with the current state of ice sheet mass balance. In addition to our groups work on improving the ICESat data geolocation accuracy for change detection, we have also developed unique approaches in GRACE data processing and mass change recovery. Specifically, we have developed a capability to recover local/regional gravity changes using non-global functional representations (i.e. surface anomalies vs. global spherical harmonics) from the GRACE data *[Rowlands et al. 2002 and 2005]*. We are beginning to exploit the unique strengths within our team to process both the level 1 GRACE and ICESat data. Using unique ICESat and GRACE analysis approaches we hope to provide an improved methodology to reliably estimate mass flux over regional (e.g. large glaciers, ablation zones, etc.) and basin-wide scales. We will assess the utilization of the ICESat and GRACE data in simultaneous solutions for Antarctic and Greenland mass flux across co-observed periods.

2.6 Topographic Changes Associated with the Sumatra Earthquake

ICESat repeat-profiling detection of elevation change can substantially contribute to documenting the spatial pattern of crustal deformation caused by the December, 2004 Sumatra magnitude 9.0 earthquake and aftershocks. Preliminary modeling by Chen Ji, of the deformation pattern associated with the main event using teleseismic data shows significant deformation limited to a 450 km long section of the southern Sunda Trench, off the west coast of Sumatra (Figure 12). Most of the deformation is below sea-level; modeled on-land deformation in Sumatra is relatively small, < 1 m vertical and < 3 m horizontal, probably below ICESat detection capabilities using repeat profiles. However, based on the spatial distribution of aftershocks, the fault rupture zone extends an additional 1,000 km northward along the Sunda subduction zone. Anecdotal reports in this region from the Andaman and Nicobar Island chains describe uplift by as much as 3 m and and satellite images document uplift of island-fringing coral reef platforms above sea level. Four ICESat tracks, with cloud-free data acquired in the fall of 2003 and 2004, cross the Andaman and Nicobar Islands (Figure 12). The spatial pattern of uplift, documented by exactly repeating these profiles, will help constrain models of slip distribution on the fault plane, a key to understanding this event and future subduction zone mega-earthquakes. Repeat profiling is planned for 2005. Acquisition of these new ICESat profiles will require the greatest pointing control accuracy achievable, so as to exactly repeat the prior profiles. Also, the best-possible calibration of pointing, timing, range, and orbit biases will be needed to recover the elevation changes along these profiles at the sub-meter level.

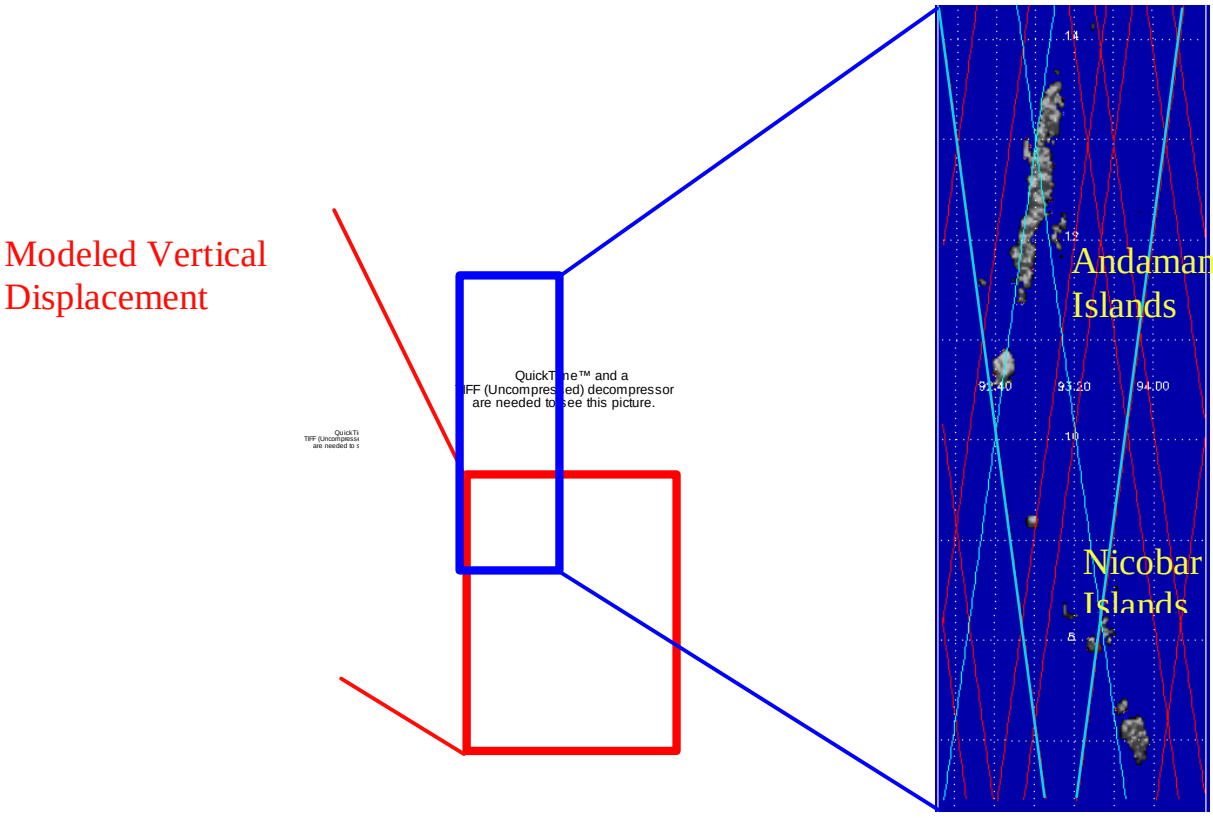

Figure 12. Locations of the M9.0 Sumatra epicenter and aftershocks along the Sunda subduction zone (center, from USGS), main event vertical displacements modeled from teleseismic data (left, from Chen Ji, Cal Tech), and locations of ICESat profiles acquired during the L2A observation period (right). Cloud-free profiles crossing islands of the Andaman and Nicobar chains are highlighted (cyan).

3. Instrument Operations Contributions

Following L1A operations, developed round-the-world scan calibration methodology to document waveform skew introduced by FOV shadowing and establish orbital variation in transmitted beam and receiver pointing (Luthcke, Harding)

Following L1A operations, contributed to revision of on-board gain algorithm to reduce the level and frequency of waveform saturation (Harding, Carabajal, Sauber)

Following L1A operations, provided Alaska examples over steep, glaciated terrain to Instrument team for revision of GLAS data acquisition algorithm (Sauber)

Following L2A operations, documented truncation of broad waveforms for areas of steep slopes and/or tall vegetation and recommended waveform compression correction which was adopted (Harding, Sauber)

Following L2A operations, identified incorrect implementation of range gating associated with off-nadir targets of opportunity causing data loss and recommended correction which was adopted (Harding)

Following L2C operations, recommended methodology for daily monitoring of gain algorithm performance and waveform saturation which was adopted (Harding, implemented by Saba)

Following L1A and L2A operations, coordinated reporting and integration of observations related to FOV offsets associated with temperature changes (Harding, Luthcke, Carabajal))

For L2 observations, coordinated targeting ICESat on calibration sites for vegetation cover and inland water (Harding, Lefsky, Carabajal)

For L3A observations, coordinated targeting ICESat on Mount St. Helens during period of renewed volcanic activity (Harding)

For L3B observations, coordinated targeting ICESat on Andaman and Nicobar Island chains to determine topographic changes (uplift, subsidence, tilting) associated with Sumatra M9.0 earthquake and aftershocks (Harding)

4. Data Processing and Visualization Contributions

Established appropriate threshold level for definition of alternate signal start and end (Harding)

Identified missing or miss-specified parameters in GLA structures including alternate signal start offset, and beam azimuth and co-elevation angles (Harding, Carabajal)

Documented and validated GLA orientation parameters and their relationship to the GLAS optical bench including track azimuth, transmit beam azimuth and co-elevation, and footprint azimuth (Carbajal, Harding)

Revised and documented alternate Gaussian waveform fitting to significantly improve representation of complex waveforms by preserving six peaks and constraining base level (Harding, implemented by Roberts)

Recommended and specified improvements to GLAS Data Visualizer, including save/restore of plot parameters and export of footprint latitude and longitude (Harding, implemented by SCF staff)

Evaluated flagging of saturated land returns and recommended revised implementation to properly identify saturated returns and provide a measure of degree of saturation (Harding, not yet implemented)

Evaluated Gaussian fitting correction for saturated returns (fit leading edge and preserve area) and identified problems with the implementation (Harding, in on-going collaboration with SCF staff)

Recommended and specified use of SRTM 90 m DEM as source to provide GLA land elevation values (Harding, Carabajal, Sauber, implemented by SCF staff but not yet included in data releases)

5. External Collaborations and Student Training

All members of the team have supported external users in their understanding and use of the ICESat data products, and have significantly contributed to the production of release notes that facilitate data use by outside collaborators and the general research community. Specifically, explanations have been provided on geolocation accuracy, the spatial and temporal coverage for land products, the definition and method of production for land and waveform product parameters, and best use of products to achieve specific objectives. Team members have also contributed to outreach efforts by presenting information on the general objectives of the mission, calibration efforts and scientific results at workshops, university seminars, and international meetings. External collaborations, all of which include student training in the use of ICESat data, resulting in presentations at scientific conferences include:

1. *Darius Mitchell, Case Western Reserve*, EGU-AGU presentation, Mitchell, D. J. Sauber, D. Harding, C. Carabajal, W. Krabill, S. Manizade, J. Bufton, 2003, Expected ICESat measurement

of glacier elevation change, Geophysical Research Abstracts, v. 5, 04153, European Geophysical Society.

2. *Katy Wiest, University of Texas at El Paso,* AGU presentation, Wiest, K.R., J.M. Sauber, A. A. Velasco, D.L. Doser, and J.M. Hurtado, 2004, The relationships between earthquakes, faults and recent glacier fluctuations in southern Alaska, *Eos Trans. AGU, 85(47),* Fall Meet. Suppl. Abstract S53A-0179.

3. *Reiji Muskett, University of Alaska*, IGARSS presentation, Muskett, R., C. Lingle, R. Guritz, D. Atwood, J. Sauber, R. Gens, N. LaBell-Hamer, and B. Kerrin, 2004, DEM control in Arctic Alaska with ICESat altimetry.

4. *Michael Lefsky, Colorado State University,* AGU presentation, Lefsky, M.A., Harding, D.J., Warren, W.B., and Keller, M., 2004, Estimating forest canopy height from Geoscience Laser Altimeter System waveforms and Shuttle Radar Topography Mission digital elevation models, *Eos Trans. AGU, 85*(47), Fall Meet. Suppl., Abstract C21B-07.

6. References

Arendt, A.A., K.A. Echemeyer, W.D. Harrison, C.S. Lingle, and V. B. Valentine, 2002, Rapid wastage of Alaska glaciers and their contribution to rising sea level, *Science*, 297, 382-386.

Carabajal, C.C., D.J. Harding, J.L. Bufton, S.B. Luthcke and D.D. Rowlands, 2003, ICESat Geolocation and Land Products Validation: Laser Altimetry Profile and Waveform Matching, International Archives of Photogrammetry, Proceedings of the ISPRS workshop on 3D mapping from InSAR and Lidar, WG I/3-WGII/2, Portland OR.

Carabajal, C.C., and D.J. Harding, 2005, ICESat Validation of SRTM C-Band Digital Elevation Models, *Geophysical Research Letters*, ICESat topical issue, submitted.

Echemeyer et al., 1996, Airborne surface profiling of glaciers: A case study in Alaska, *Journal of Galciology*, 42(142), 538-547.

Harding, D.J., and Carabajal, C.C., 2005, Validation of ICESat Waveform Observations of Within-footprint Canopy Structure and Ground Relief, *Geophysical Research Letters*, ICESat topical issue, submitted.

Harding, D.J., and Jasinski, M.F., 2004, ICESat Observations of Inland Surface Water Stage, Slope, and Extent: a new Method for Hydrologic Monitoring, *Eos Trans. AGU, 85*(47), Fall Meet. Suppl., Abstract C21B-05.

Lefsky, M.A., W.B. Cohen, D.J. Harding, G.G. Parker, S.A. Acker, and S.T. Gower, 2002, Lidar remote sensing of aboveground biomass in three biomes, *Global Ecology and Biogeography*, 11(5): 393-399.

Lefsky, M.A., Harding, D.J., Cohen, W.B., Keller, M., Carabajal, C.C., 2005, Estimating forest canopy height and aboveground bimass from ICESat waveforms and Shuttle Radar Topography Mission digital elevation models, *Geophysical Research Letters*, ICESat topical issue, submitted.

Luthcke, S.B., Carabajal, C.C and D.D. Rowlands, 2002, Enhanced Geolocation of Spaceborne Laser Altimeter Surface Returns: Parameter Calibration from the Simultaneious Reduction of

Altimeter Range and Navigation Tracking data, *Journal of Geodynamics*, Vol. 34, No. 3-4, pp. 447-475.

Luthcke, S.B., D.D. Rowlands, F.G. Lemoine, N.P. Zelensky and T.A. Williams, 2003, GPS-based Precision Orbit Determination for a New Era of Altimeter Satellites: Jason-1 and ICESat, Proceedings from the Flight Mechanics Symposium, NASA Goddard Space Flight Center

Luthcke, S.B., D.D. Rowlands, C.C. Carabajal, D.J. Harding, J.L. Bufton and T.A. Williams, 2003, ICESat Laser Altimeter Pointing, Ranging and Timing Calibration From Integrated Residual Analysis: A Summary of Early Mission Results, Proceedings from the Flight Mechanics Symposium, NASA Goddard Space Flight Center.

Luthcke, S.B., Rowlands, D.D., McCarthy, J.J., Stoneking, E. and Pavlis, D.E., 2000, Spaceborne Laser Altimeter Pointing Bias Calibration From Range Residual Analysis, *Journal of Spacecraft and Rockets*, Vol. 37, No. 3, pp. 374-384.

Luthcke et al., 2005, Calibration and reduction of ICESat geolocation errors and the impact on change detection, *Geophysical Research Letters*, ICESat topical issue, submitted.

Ramage, J. M., and B. L. Isacks, 2003, Interannual variations of snowmelt and refreeze timing on southeast-Alaska icefields, U.S.A., *Journal of Galciology*, 49(164), 102-116.

Rowlands, D. D., C. C. Carabajal, S. B. Luthcke, D. J. Harding, J. M. Sauber, and J. L. Bufton, 2000, Satellite Laser Altimetry: On-Orbit Calibration Techniques for Precise Geolocation, *The Review of Laser Engineering*, Vol. 28, No. 12, pp. 796-803.

Rowlands, D.D., R.D. Ray, D.S. Chinn, F.G. Lemoine, 2002, Short-arc analysis of intersatellite tracking data in a gravity mapping mission, *Journal of Geodesy*, 76, pp. 307-316.

Rowlands, D.D., S.B. Luthcke, S.M. Klosko, F.G.R. Lemoine, D.S. Chinn, J.J. McCarthy, C.M. Cox, O.B. Anderson, 2005, Resolving mass flux at high spatial and temporal resolution: 'mascon' estimation using GRACE intersatellite measurements, *Geophysical Research Letters*, in press.

Sauber, J., G. Plafker, B.F. Molnia, and M.A. Bryant, 2000, Crustal deformation associated with glacial fluctuations in the eastern Chugach Mountains, Alaska, *Journal of Geophysical Research*, 105(B4), 8055-8077.

Sauber, J. M., and B. Molnia, 2004, Glacier ice mass fluctuations and fault instability in tectonically active southern Alaska, *Global and Planetary Change*, Topical Issue "Ice Sheets and Neotectonics", eds. T.S. James, T.H. Jacka, A. Morelli, and R. Dietrick, 42, 279-294.

Sauber, J., B. Molnia, and D. Mitchell, 2003, ICESat Observations of southern Alaska Glaciers, *Eos Trans. AGU*, 84(46), Fall Meeting Suppl., Abstract C31D-07.

Sauber, J., B. F. Molnia, S. Luthcke, D. Rowlands, D. Harding, C. Carabajal, J.M. Hurtado, and G. Spada, 2004, Southern Alaska glaciers: spatial and temporal variations in ice volume, *Eos. Trans. AGU*, 85(47), Fall Meet. Suppl., Abstract, C22A-03.

Sauber, J., B. Molnia, C. Carabajal, S. Luthcke, and R. Muskett, 2005, Elevation change (2000-2004) on the Malaspina Glacier, Alaska, *Geophysical Research Letters*, ICESat topical issue, submitted.

Wiest, K.R., J.M. Sauber, A. A. Velasco, D.L. Doser, and J.M. Hurtado, 2004, The relationships between earthquakes, faults and recent glacier fluctuations in southern Alaska, *Eos Trans. AGU, 85(47)*, Fall Meet. Suppl. Abstract S53A-0179.